Saharan Dust PLDR, Using Realistic Shapes, Sizes and Refractive Indices

Alexandra Tsekeri[a], Anna Gialitaki,[a,b] Josef Gasteiger[c], Natalia Kustova[d], Alexander Konoshonkin[d], Maxim A. Yurkin[e], Thanasis Georgiou[a,f], Johanne Ekue[a,f], Spyridon Metallinos[a], Niki Asimakopoulou[a], Peristera Paschou[a], Nikolaos Siomos[g], Anna Kampouri[a], Maria Tsichla[a,h], Eleni Marinou[a], Maria Kezoudi[i], Franco Marenco[i], Alkistis Papetta[i], Sudharaj Aryasree[j], Konrad Kandler[j], Moritz Haarig[k], Athena Floutsi[k], Holger Baars[k], Amin Nehrir[l], James Collins[l], Ewan Crosbie[l], Rory Barton-Grimley[l], Edward P. Nowottnick[m], and Vassilis Amiridis[a]

[a]IAASARS, National Observatory of Athens, Athens, Greece
[b]School of Physics and Astronomy, Earth Observation Science Group, University of Leicester, UK
[c] Hamtec Consulting GmbH, EUMETSAT, Darmstadt, Germany
[d]V. E. Zuev Institute of Atmospheric Optics SB RAS, Tomsk, Russia
[e]Université Rouen Normandie, INSA Rouen Normandie, CNRS, CORIA UMR 6614, Rouen, France
[f]Physics Department, Aristotle University of Thessaloniki, Thessaloniki, Greece
[g] Chair of Experimental Meteorology, Faculty of Physics, Ludwig-Maximilians-Universität München, 80539, Germany
[h]Environmental Chemical Processes Laboratory, Department of Chemistry, University of Crete, Greece
[i]Climate and Atmosphere research Centre (CARE-C), The Cyprus Institute, Nicosia, Cyprus
[j]Institute of Applied Geosciences, Technical University of Darmstadt, Darmstadt, Germany
[k]Leibniz Institute for Tropospheric Research, Leipzig, Germany
[l]NASA Langley Research Center, Hampton, VA
[m]NASA Goddard Space Flight Center, Greenbelt, Maryland

Abstract: The remote sensing of airborne dust particles still faces barriers due to uncertainties in their optical properties, for which the calculations in the full UV-SWIR spectral range are challenging, mainly due to the dust particle irregular shapes and large sizes. Especially the backscatter properties are associated with high uncertainties, limiting the potential of lidar applications for desert dust. Our work investigates calculations of the Particle Linear Depolarization Ratio (PLDR) for Saharan dust particles with realistic irregular shapes, large sizes, and refractive indices (RIs). The PLDR at 1064 nm is 30-40%, calculated with high certainty, and in good agreement with lidar field observations. The PLDR at 355 and 532 nm are provided as well, however associated with high uncertainties. Using realistic microphysical properties, this work sets the baselines for dust in lidar applications allowing, e.g., investigations of the mixing state of dust in the atmosphere.

1. Introduction

The accurate modelling of the dust optical properties is an open scientific question, particularly for the backscatter, mainly due to the irregular shapes and large sizes of the particles. Scattering calculations considering realistic irregular shapes are computationally costly, and as of yet, are provided for (cross-section-equivalent) size parameters up to 30, only from the MOPSMAP scattering database [1], for the realistic irregular shapes presented in Gasteiger et al. [2] (Fig. 1), using the ADDA code [3]. For lidar applications, MOPSMAP does not fully cover the size range of airborne dust particles, even for the larger (at least for the majority of lidar systems) wavelength of 1064 nm.

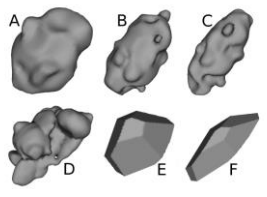

Figure 1. Realistic irregular shapes used for scattering calculations herein *(Source: Gasteiger et al., [2])*

Scattering calculations covering the full range of dust sizes and RIs are provided in the literature for simpler non-spherical shapes: spheroids [4], ellipsoids [5], super-ellipsoids [6], and irregular hexahedrals [7]. Even though these models are quite valuable for calculations across the full wavelength spectrum (e.g. for dust radiative forcing studies [8]), their limitations in reproducing the full suite of dust backscattering properties limits their applicability for dust lidar studies.

Towards constructing a scattering database for realistic dust particles, to be used for lidar applications, we have **extended the ADDA/MOPSMAP calculations to size parameters up to 68, for four dust refractive indices ((1.48-1.6) + i(0-0.002))**. These "ADDA/NOA calculations" cover the size range of airborne dust particles for backscatter at 1064 nm (Fig. 2e), enabling us to calculate accurately the PLDR at 1064 nm (Sect. 2).

For calculations at shorter wavelengths of 355 and 532 nm, and size parameters >70, ADDA calculations are challenging even for high-performance computing (HPC) systems, due to the large number of dipoles and orientations needed, and the very slow convergence of the iterative solver. Thus, in order to formulate a complete (back)scattering database for dust for wavelengths of 355, 532 and 1064 nm, we further investigate the applicability of the much faster Physical Optics (PO) approximation [9] for dust particles with faceted shapes (Sect. 3).

2. Calculation of PLDR at 1064 nm

Figure 2a shows the PLDR for single particles, for shapes A, B, C and D (Fig. 1), in random orientation, from ADDA/NOA calculations (size parameter up to 68). Shapes E and F are excluded from our analysis, since in-situ observations have shown that particles with flat surfaces are rare (<1%) in Saharan dust samples, and their flat surfaces are much smaller, resembling surface roughness. A more detailed view is provided for shape A in Fig. 2b-d, for the PLDR (Eqn. 1), and the P_{11} and P_{22} elements of the (normalized) backscatter matrix. The ADDA/MOPSMAP calculations (size parameter up to 30) are also shown.

$$PLDR = 100\frac{P_{11} - P_{22}}{P_{11} + P_{22}} \quad (1)$$

Climatological dust size distributions for the Saharan Air Layer (SAL) [10] are also shown in Fig. 2e, with their size range to be well-covered by the ADDA/NOA calculations.

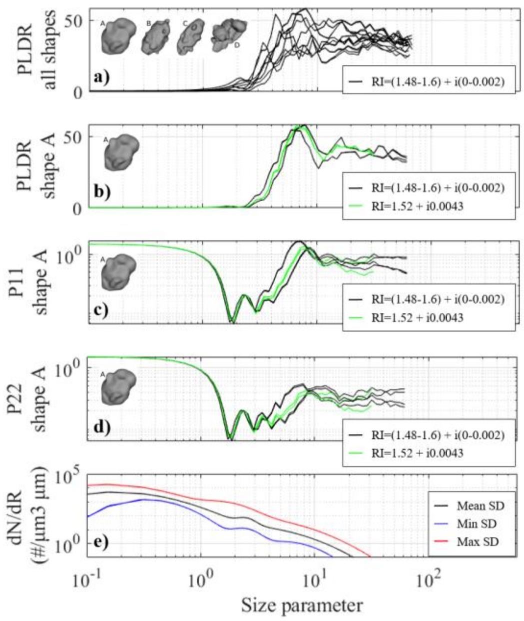

Figure 2. a) PLDR for single particles with shapes A-D (Fig. 1). b) c) and d) show the single-particle calculations specifically for shape A: the PLDR, P_{11} and P_{22}, respectively. Black lines denote the ADDA/NOA calculations, and green lines the ADDA/MOPSMAP calculations. e) Climatological minimum/mean/maximum dust size distributions $\left(\frac{dN}{dR}\right)$ measured in-situ in the SAL, during the AER-D campaign [10].

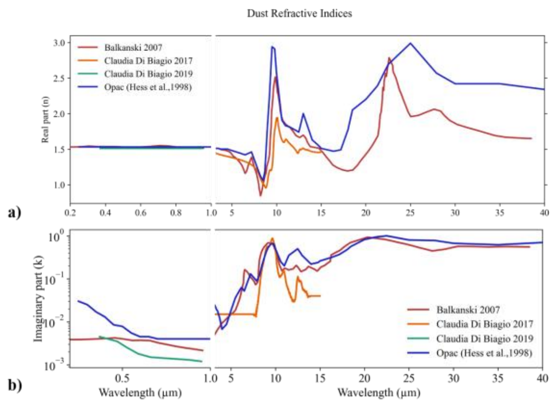

Figure 3. a) Real and b) imaginary part of the RI of dust particles, based on various studies in the literature.

More specifically, for the PLDR calculations at 1064 nm we have used RI=(1.48-1.6) + i(0-0.002), covering the minimum/mean imaginary part of RI at 1064 nm, as reported from various studies in the literature (Fig. 3b). We have also used RI=1.52+i(0-0.0043) provided by the ADDA/MOPSMAP database, in order to take into account the climatological mean for the real part of the RI and the minimum/maximum imaginary part of the RI at 1064 nm (Fig. 3). Both provide similar results, with ADDA/MOPSMAP to be associated though with higher uncertainty, due to its limited size range.

For calculations considering dust particle ensembles, we generated different shape combinations (Fig. 4b), based on the percentages provided by in-situ measurements in SAL during the ASKOS campaign [11] (Fig. 4a).

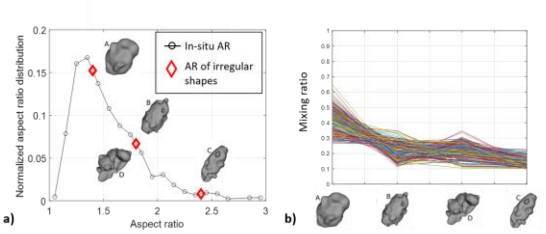

Figure 4. a) In-situ measurements in SAL of the aspect ratio of dust particles during the ASKOS campaign [11], corresponding to the shapes A-D, as shown in the plot. b) Different (number) mixing ratios for particles with shapes A-D, used for our calculations.

Taking all the above into account, regarding the climatological ranges for the realistic size, RI and shape of airborne dust in SAL, we calculated the **PLDR at 1064 nm for dust particles at 30-40%** (Fig. 7), with the values presenting small differences between the climatological mean/min/max size distributions.

3. Extend calculations for PLDR at 355 and 532 nm (larger particle sizes)

In order to investigate the PLDR at 355 and 532 nm, we **extend the scattering calculations to larger sizes, utilizing the PO approximation** This is work in progress, entailing up to now only the faceted shape F (Fig. 1), since PO is applicable only for faceted particles [9] (the next step is to apply PO to shapes A-D, after reproducing them with small facets). Figure 5 shows first results: in case of no absorption (RI=1.6+i0) the PLDR is constant for the larger particles at size parameters 60-300; for absorbing particles (even for small absorption with RI=1.6+i0.002) the PLDR drops after size parameter 60, and becomes zero at size parameter of 200.

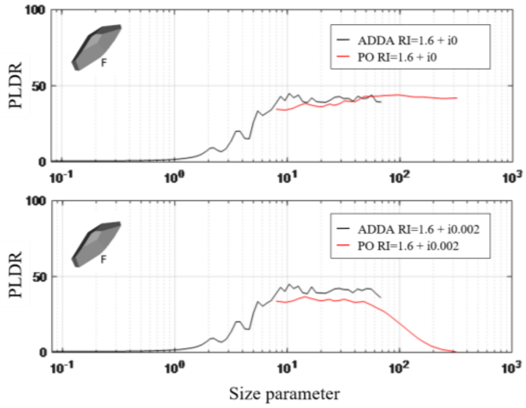

Figure 5. PLDR comparison for ADDA/NOA (black) and PO (red), for shape F (Fig. 1), for RI=1.6+i0 (top) and RI=1.6+i0.002 (bottom).

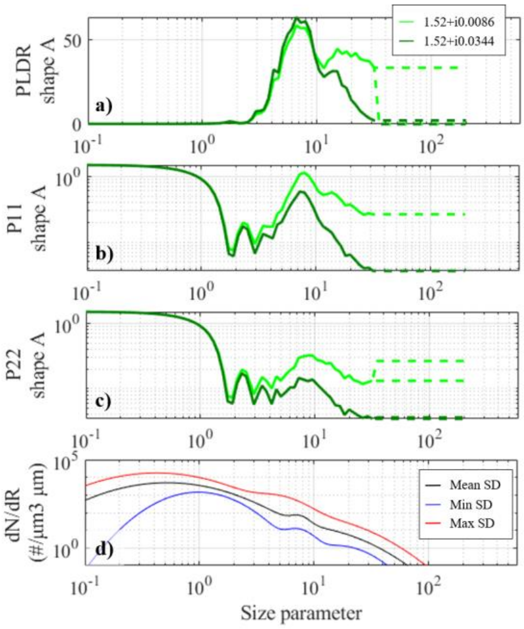

Figure 6. Example of extending ADDA/MOPSMAP scattering calculations at 355 nm.

These results are preliminary, but they show that **the PLDR of single particles with large size remains constant (at ~40%) or drops at 0**%. Based on this finding, we extend the ADDA/MOPSMAP scattering data so as the PLDR for size parameter>30 is either constant (equal to its value at size parameter 30) or 0%. To do so, we consider that P_{11} is constant for size parameter≥30 and we derive the corresponding P_{22} from Eqn. 1, as shown in Fig. 6 for the calculations at 355 nm. Then we perform the calculations considering the size distributions and shape as shown in Fig. 6 for the calculations at 355 nm. Then we perform the calculations considering the size distributions and shape mixtures discussed in Sect. 2, using the climatological RIs for 355 nm (RI=1.52+i(0.0043-0.0344)) and for 532 nm (RI=1.52+i(0.00215-0.0086)) (Fig. 3). The results for the PLDR at 355 and 532 nm are shown in Fig. 7.

Using this methodology, **we do not derive the exact values of the PLDR at 355 and 532 nm, but a range of "acceptable" values, based on the clear tendencies provided by PO for the PLDR of particles with large sizes** (Fig. 5). Although the range of values, especially for the PLDR at 355 nm, is quite large for practical lidar applications, these results are still informative: it is interesting to note that observations assigned to "dust" in the literature [12] (black frames in Fig. 7) are not possible based on our calculations, since they would imply that the single-particle PLDR for large sizes would be negative.

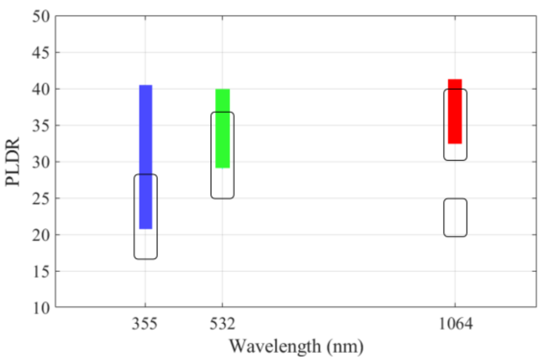

Figure 7. Saharan dust PLDR at 355 (blue) and 532 nm (green), based on extended ADDA/MOPSMAP scattering calculations. The PLDR at 1064 nm (red) is calculated based on the ADDA/NOA scattering calculations (not extended, with high accuracy). The black frames show the corresponding values for Saharan dust from the literature [12] for 355 and 532nm, and for 1064 nm from ASKOS campaign [11] with the PollyXT Raman-polarization lidar [13] and with the NASA Langley HALO HSRL, along with observations in Athens, Greece, with the WALL-E lidar [14].

4. Insights regarding the dust mixing state

Figure 7 shows lidar observations reported in the literature that, compared to our calculations, provide also smaller values for the PLDR at 355, 532 nm [12], and for 1064 nm [13]. The low-PLDR values may be reproduced if we take into account possible mixing of airborne Saharan dust with other aerosol types, as pollution or even marine particles. Since the **PLDR at 1064 nm** is derived herein with a high certainty, it **may be a valuable tool for studying the mixing state of Saharan dust in the atmosphere**, as has also been suggested in previous studies [15].

5. References

[1] J. Gasteiger and M. Wiegner, Geosci. Model Dev., **11**, 2739 (2018).

[2] J.M. Gasteiger, et al., Tellus B, **63**, 725 (2011).

[3] M.A. Yurkin and A. G., Hoekstra, J. Quant. Spectrosc. Radiat. **112**, 2234 (2011).

[4] O. Dubovik, et al., J. Geophys. Res., **111**, D11208 (2006).

[5] Y. Huang, et al., Atmos. Chem. Phys., **23**, 2557–2577, (2023).

[6] L. Bi, et al., Opt. Express, **26**, 1726-1742, (2018).

[7] M. Saito, et al., J. of Atm. Sciences, **78**, 2089–2111, (2021).

[8] I. Fountoulakis, et al., Atmos. Chem. Phys., 24, 4915–4948, (2024).

[9] A. Konoshonkin, et al., J. Quant. Spectrosc. Radiat. Transf. 195, 132 (2017).

[10] C. Ryder, et al., Atmos. Chem. Phys., **19**, 15353–15376, (2019).

[11] E. Marinou, et al., p. 200 in Environmental Sciences Proceedings 26 (2023).

[12] A.A. Floutsi, et al., Atmos. Meas. Tech., **16**, 2353–2379, (2023).

[13] H. Gebauer, et al., Atmos. Chem. Phys., **26**, 3439–3465, (2026).

[14] A. Tsekeri, et al., Atmos. Meas. Tech., **14**, 7453–7474, (2021).

[15] N. Sugimoto, and C.H. Lee, Applied optics, **45**, 7468–7474, (2006).

Acknowledgements:

This work has been financially supported by the Obs3RvE (Optimising 3D RT Earthcare product using geostationary observations and AI) project, funded from the European Space Agency under Contract No. 4000147848/25/I/AG, the CERTAINTY project (Grant Agreement 101137680) funded by Horizon Europe program. It is also based upon work from COST Action EARLICOST, CA24135, supported by COST (European Cooperation in Science and Technology). The calculations using the PO approximation were supported by the Ministry of Science and Higher Education of the Russian Federation (V.E. Zuev Institute of Atmospheric Optics SB RAS). MYu acknowledges support of the Normandy Region (project RADDAERO). AT would like to acknowledge COST Action HARMONIA (International network for harmonization of atmospheric aerosol retrievals from ground-based photometers), CA21119, supported by COST (European Cooperation in Science and Technology). We acknowledge the Dust-DN project, funded by the European Union under the Marie Skłodowska-Curie Actions (grant agreement 101168425), and by the corresponding national agencies of the United Kingdom (UKRI) and Switzerland (SERI).